Robótica de Manipulação
Departamento de Engenharia Mecânica

Inverse Kinematics of Robotic Manipulators

Course Notes

André S. Carvalho, Jorge M. Martins

{andre.s.carvalho,jorgemartins}@tecnico.ulisboa.pt

Universidade de Lisboa, Instituto Superior Técnico,
Av. Rovisco Pais, 1049-001 Lisboa, Portugal.

version 1.0

April, 2020

...geometry is the art of reasoning well from badly drawn figures;

Henri Poincaré, *Analysis Situs* (1895)

1 Introduction

In the context of robotic manipulators, the inverse kinematics problem is defined as the problem of determining the joint coordinates which achieve a given Cartesian configuration (pose) of the end-effector's frame. The solution of this problem is motivated by the fact that objects in the manipulator's workspace are usually referenced, with respect to said Cartesian frames, using length and angle measurements. Thus, the solution of the inverse kinematics problem is indeed the most natural way of specifying the manipulator's motions, in order to achieve a given task.

Contrary to the direct kinematics problem, which consists on the calculation of the end-effector's pose from the joint coordinates, the inverse one does not have a systematic procedure, oftentimes requiring a leap forward in the understanding of the manipulator's geometry in order to formulate its solution. With that in mind, the inverse kinematics solution of commercial robots is a central issue, which is also quite informative in determining the manipulator's internal and boundary singularities. Therefore, more often than not, it is the first topic which is searched for in the literature when addressing a specific manipulator. In this regard there is an extensive body of work with differing approaches for a multitude of manipulators.

To illustrate the motivation for the present document, it is also noted that when perusing these solutions one also encounters differing styles of notation and conventions. Thus, adding to the demanding nature of the problem, it may indeed be a challenging task to fully understand the geometry of the solution and, more importantly, generalize this knowledge to the solution of inverse kinematics problems in other mechanisms. Moreover, although these solutions might arise from geometrical insight, they are often presented in an analytical format which hinders one's visual experience of the world [1]. With that in mind, the goal of this document is to provide inverse kinematics solutions of systems with incremental complexity, following a geometrical approach. Thus, it is hoped that from this essay the reader will not only be able to understand the geometrical construction of inverse kinematics solutions and extrapolate these ideas to the solution of a variety of mechanisms, but also employ their geometrical constructions to the understanding of direct kinematics problems in an insightful fashion. This document is intended to complement the direct kinematics of robotic manipulators and the Denavit-Hartenberg convention [3, §2].

This document is organized as follows. In §2 the direct kinematics of robotic manipulator's is briefly review and the nomenclature for the ensuing illustrations is outlined, before proceeding to the inverse kinematics solutions of increasing complexity. Thus, planar geometries are discussed in §3 through §6, before the spatial arrangements discussed in §7 through §9.

2 Preliminaries

As stated in the introduction, the Denavit-Hartenberg (D-H) convention is here followed to define the manipulator's frames and their relative motion. Apart from this, a basic understanding of trigonometry is needed, including expressing trigonometric functions in terms of angles in the first quadrant [2, §6.5.6], and knowledge their inverse counterparts, such as the two-argument inverse tangent function [3, §2.4.1], $\vartheta = \arctan(\mathrm{s}_\vartheta, \mathrm{c}_\vartheta)$. In this chapter the D-H convention is first reviewed, followed by an introduction to the graphical notation that will be used throughout this essay.

A robotic manipulator may be considered as an open kinematic chain of $n+1$ rigid bodies, the links, connected by n joints of one degree of freedom, either revolute or prismatic. The joints represent lower kinematic pairs of one degree of freedom, and in [4] it is shown that for these joints, by appropriately attaching the reference frames to the two connecting links, the number of parameters which are required to describe their relative position and orientation may be reduced from six to four parameters.

According to the D-H convention, illustrated in Figure 2.1(a), the order of the four transformations is defined through a translation d_i along $\boldsymbol{z}_{i-1}$, followed by a rotation ϑ_i about $\boldsymbol{z}_{i-1}$, followed by a translation a_i along the rotated $\boldsymbol{x}_{i-1}$ axis, $\boldsymbol{x}'_i$, and finally followed by a rotation α_i about $\boldsymbol{x}'_i$. Here, frame i' was introduced as an intermediate frame between frames $i-1$ and i. These transformations define the relative position and orientation of the manipulator's links as a function of the joint coordinates. In this regard, link i is the rigid body to which frame i has been attached.

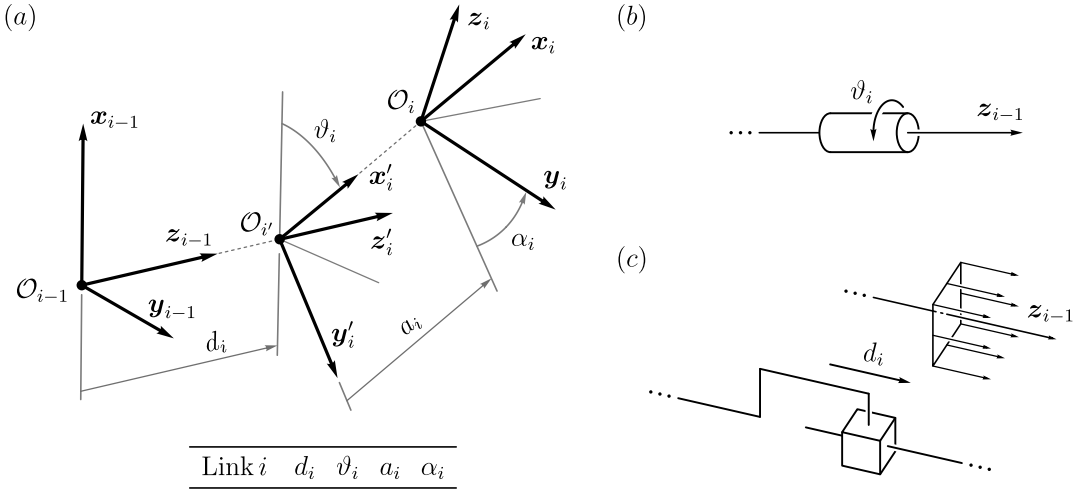

Figure 2.1: (a) D-H transformation for link i. (b) Revolute joint i. (c) Prismatic joint i.

The joint coordinates of the manipulator can be illustrated through a joint diagram, where two types of joints can be employed to represent any possible motion for the manipulator's end-effector. A revolute joint is illustrated as a cylinder, as in Figure 2.1(b), defining the axis of

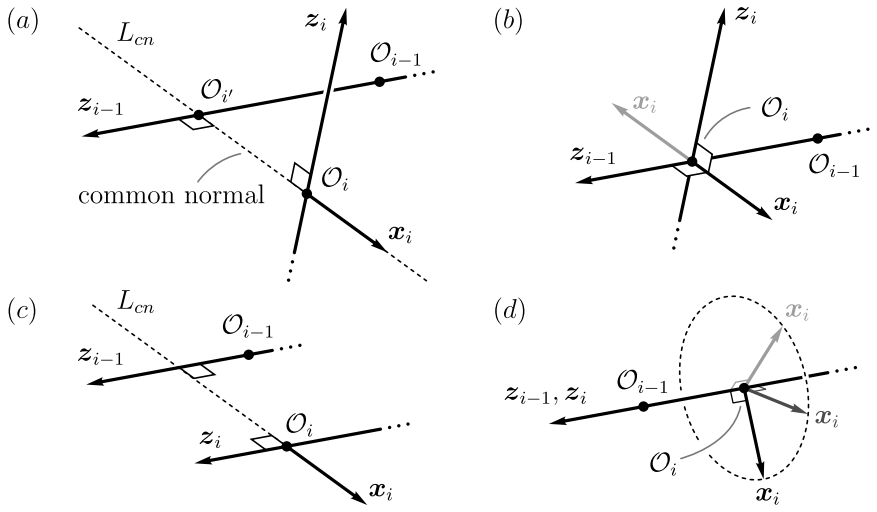

Figure 2.2: Possible configurations for axes $\boldsymbol{z}_{i-1}$ and $\boldsymbol{z}_i$, as detailed in Algorithm 1. Here, in (a,c), L_{cn} is the common normal to $\boldsymbol{z}_{i-1}$ and $\boldsymbol{z}_i$, denoting the line perpendicular to both axes.

rotation, $\boldsymbol{z}_{i-1}$, for joint i. A prismatic joint is illustrated as a cube, as in Figure 2.1(c), defining a displacement field for the joint. An arbitrary axis of translation $\boldsymbol{z}_{i-1}$ in that field can then be chosen to define the translation joint i. Following the joint diagram of the manipulator, the reference frames for each link can then be constructed. The systematic construction of said D-H frames and their corresponding table of parameters can be followed from Algorithm 1 and Figure 2.2.

Once the D-H parameters are determined, the homogeneous transformation matrices between each of the frames illustrated in Figure 2.1(a) can be gathered into

$$\boldsymbol{A}_{i'}^{i-1} = \begin{pmatrix} \mathrm{c}_{\vartheta_i} & -\mathrm{s}_{\vartheta_i} & 0 & 0 \\ \mathrm{s}_{\vartheta_i} & \mathrm{c}_{\vartheta_i} & 0 & 0 \\ 0 & 0 & 1 & d_i \\ 0 & 0 & 0 & 1 \end{pmatrix} \quad , \quad \boldsymbol{A}_{i}^{i'} = \begin{pmatrix} 1 & 0 & 0 & a_i \\ 0 & \mathrm{c}_{\alpha_i} & -\mathrm{s}_{\alpha_i} & 0 \\ 0 & \mathrm{s}_{\alpha_i} & \mathrm{c}_{\alpha_i} & 0 \\ 0 & 0 & 0 & 1 \end{pmatrix} , \tag{2.1}$$

to write the homogeneous transformations between frames i and $i-1$,

$$\boldsymbol{A}_{i}^{i-1} = \boldsymbol{A}_{i'}^{i-1}\boldsymbol{A}_{i}^{i'} = \begin{pmatrix} \mathrm{c}_{\vartheta_i} & -\mathrm{s}_{\vartheta_i}\,\mathrm{c}_{\alpha_i} & \mathrm{s}_{\vartheta_i}\,\mathrm{s}_{\alpha_i} & a_i\,\mathrm{c}_{\vartheta_i} \\ \mathrm{s}_{\vartheta_i} & \mathrm{c}_{\vartheta_i}\,\mathrm{c}_{\alpha_i} & -\mathrm{c}_{\vartheta_i}\,\mathrm{s}_{\alpha_i} & a_i\,\mathrm{s}_{\vartheta_i} \\ 0 & \mathrm{s}_{\alpha_i} & \mathrm{c}_{\alpha_i} & d_i \\ 0 & 0 & 0 & 1 \end{pmatrix} , \tag{2.2}$$

further allowing to systematically determine the direct kinematics of the manipulator, as

$$\boldsymbol{A}_{n}^{o} = \begin{pmatrix} \boldsymbol{R}_{n}^{o} & \boldsymbol{r}_{o,n}^{o} \\ \boldsymbol{0}^{\intercal} & 1 \end{pmatrix} = \boldsymbol{A}_{1}^{o}\,\boldsymbol{A}_{2}^{1} \ldots \boldsymbol{A}_{n}^{n-1} . \tag{2.3}$$

With respect to the present notation, $\boldsymbol{R}_{\beta}^{\alpha} = (\boldsymbol{x}_{\beta}^{\alpha}\ \boldsymbol{y}_{\beta}^{\alpha}\ \boldsymbol{z}_{\beta}^{\alpha})$ denotes the rotation between frames β and α, where its columns are the versors of frame β expressed in frame α, while $\boldsymbol{r}_{\alpha,\beta}^{\gamma}$ denotes

Algorithm 1 Graphical construction of the Denavit-Hartenberg reference frames

$n \leftarrow$ degrees of freedom ▷ n joints connecting $n+1$ bodies
for $i = 0$ to $n-1$ **do**
    $\boldsymbol{z}_i \leftarrow$ Define axis $\boldsymbol{z}_i$ according to the type of joint $i+1$ ▷ Figures 2.1(b,c)
end for
if joint 1 is revolute **then** ▷ Define the origin of frame 0
    $\mathcal{O}_o \leftarrow$ Choose $\mathcal{O}_o$ anywhere along $\boldsymbol{z}_o$
else if joint 1 is prismatic **then**
    $\mathcal{O}_o \leftarrow$ Choose $\mathcal{O}_o$ anywhere in space
end if
$\boldsymbol{x}_o$, $\boldsymbol{y}_o \leftarrow$ Choose $\boldsymbol{x}_o$ and $\boldsymbol{y}_o$ to form a right-handed frame with $\boldsymbol{z}_o$
for $i = 1$ to $n-1$ **do**
    if $\boldsymbol{z}_{i-1}$ and $\boldsymbol{z}_i$ do not intersect **then** ▷ Figures 2.2(a,c)
        if $\boldsymbol{z}_{i-1}$ and $\boldsymbol{z}_i$ are parallel **then** ▷ Figure 2.2(c)
            $\mathcal{O}_i \leftarrow$ Choose $\mathcal{O}_i$ anywhere along $\boldsymbol{z}_i$
            $L_{cn} \leftarrow$ Locate the common normal passing through $\mathcal{O}_i$
            $\mathcal{O}_{i'} \leftarrow$ Locate $\mathcal{O}_{i'}$ at the intersection between $\boldsymbol{z}_{i-1}$ and L_{cn}
        else ▷ Figure 2.2(a)
            $L_{cn} \leftarrow$ Locate the common normal
            $\mathcal{O}_{i'}$, $\mathcal{O}_i \leftarrow$ Locate $\mathcal{O}_{i'}$, $\mathcal{O}_i$ at the intersection between L_{cn} and $\boldsymbol{z}_{i-1}$, $\boldsymbol{z}_i$
        end if
        $\boldsymbol{x}_i \leftarrow$ Define $\boldsymbol{x}_i$ along the common normal, oriented from $\mathcal{O}_{i'}$ to $\mathcal{O}_i$
    else if $\boldsymbol{z}_{i-1}$ and $\boldsymbol{z}_i$ intersect **then** ▷ Figures 2.2(b,d)
        if $\boldsymbol{z}_{i-1}$ and $\boldsymbol{z}_i$ are collinear **then** ▷ Figures 2.2(d)
            $\mathcal{O}_i \leftarrow$ Choose $\mathcal{O}_i$ anywhere along $\boldsymbol{z}_i$
            $\boldsymbol{x}_i \leftarrow$ Choose $\boldsymbol{x}_i$ such that it is orthogonal to $\boldsymbol{z}_i$ ▷ Infinite solutions
        else ▷ Figures 2.2(b)
            $\mathcal{O}_i \leftarrow$ Locate $\mathcal{O}_i$ at the intersection between $\boldsymbol{z}_{i-1}$ and $\boldsymbol{z}_i$
            $\boldsymbol{x}_i \leftarrow$ Choose $\boldsymbol{x}_i$ such that it is orthogonal to both $\boldsymbol{z}_{i-1}$ and $\boldsymbol{z}_i$ ▷ Two Solutions
        end if
    end if
    Link $i \leftarrow d_i$, ϑ_i, a_i, α_i ▷ Populate D-H table according to Figure 2.1(a)
    $\boldsymbol{y}_i \leftarrow \boldsymbol{z}_i \times \boldsymbol{x}_i$ ▷ Define $\boldsymbol{y}_i$ to form right-handed frame
end for
$\boldsymbol{x}_n$, $\boldsymbol{y}_n$, $\boldsymbol{z}_n \leftarrow$ Choose frame n in a way which is consistent with the D-H transformation in Figure 2.1(a)

the vector connecting the origin of frame α to the origin of frame β, with coordinates expressed in frame γ. Moreover, the composition of rotations and displacements can be summarized by the composition of two arbitrary homogeneous transformations, as in

$$\boldsymbol{A}_{\sigma}^{\alpha} = \boldsymbol{A}_{\beta}^{\alpha}\,\boldsymbol{A}_{\sigma}^{\beta} = \begin{pmatrix} \boldsymbol{R}_{\beta}^{\alpha} & \boldsymbol{r}_{\alpha,\beta}^{\alpha} \\ \boldsymbol{0}^{\intercal} & 1 \end{pmatrix} \begin{pmatrix} \boldsymbol{R}_{\sigma}^{\beta} & \boldsymbol{r}_{\beta,\sigma}^{\beta} \\ \boldsymbol{0}^{\intercal} & 1 \end{pmatrix} . \tag{2.4}$$

To then compose the rotations and displacements as follows,

$$\boldsymbol{A}_{\sigma}^{\alpha} = \begin{pmatrix} \boldsymbol{R}_{\beta}^{\alpha}\,\boldsymbol{R}_{\sigma}^{\beta} & \boldsymbol{r}_{\alpha,\beta}^{\alpha} + \boldsymbol{R}_{\beta}^{\alpha}\,\boldsymbol{r}_{\beta,\sigma}^{\beta} \\ \boldsymbol{0}^{\intercal} & 1 \end{pmatrix} = \begin{pmatrix} \boldsymbol{R}_{\sigma}^{\alpha} & \boldsymbol{r}_{\alpha,\beta}^{\alpha} + \boldsymbol{r}_{\beta,\sigma}^{\alpha} \\ \boldsymbol{0}^{\intercal} & 1 \end{pmatrix} = \begin{pmatrix} \boldsymbol{R}_{\sigma}^{\alpha} & \boldsymbol{r}_{\alpha,\sigma}^{\alpha} \\ \boldsymbol{0}^{\intercal} & 1 \end{pmatrix} . \tag{2.5}$$

Finally, when the origin of a frame α is measured with respect to frame o, it is convenient to employ the following notation,

$$\boldsymbol{r}_{o,\alpha}^{\beta} \triangleq \boldsymbol{p}_{\alpha}^{\beta} . \tag{2.6}$$

Furthermore, when coordinates are expressed with respect to frame zero, this dependency is also often omitted, such as in $\boldsymbol{R}_{\beta}^{o} \triangleq \boldsymbol{R}_{\beta}$ and $\boldsymbol{p}_{\alpha}^{o} \triangleq \boldsymbol{p}_{\alpha}$. Thus,

$$\boldsymbol{p}_{\alpha}^{\beta} = \boldsymbol{R}_{\beta}^{\intercal}\,\boldsymbol{p}_{\alpha} . \tag{2.7}$$

For the ensuing graphical development of inverse kinematics, it is important to define a consistent nomenclature to notate the drawings and extract the solutions. Thus, to emphasize the notation employed in the figures, the D-H convention is followed to state that, given a joint rotation between two consecutive frames, $i-1$ and i, its direction is measured positive or negative with respect to axis $\boldsymbol{z}_{i-1}$, according to the right-hand rule, and its amplitude is measured between axes $\boldsymbol{x}_{i-1}$ and $\boldsymbol{x}_{i}$. Said joint angle is notated as ϑ_i and drawn with an arrowhead with endpoint in $\boldsymbol{x}_i$. Thus, as an example, Figure 2.3(a) shows a positive rotation, $\vartheta_2 > 0$, and Figure 2.3(b) a negative rotation, $\vartheta_2 < 0$. Angle amplitudes, such as α, β, η and γ in Figures 2.3(a,b), are notated without arrowhead and always assumed positive in the context of the drawing. Thus, allowing to express $\vartheta_2 + \alpha = \beta$ and $\eta - \vartheta_2 = \gamma$, in the respective Figures.

A similar notation is employed to measure distances. If d_i is a prismatic displacement along $\boldsymbol{z}_{i-1}$, then it is drawn with an arrowhead with endpoint in the origin of frame i'. The displacement is measured positive along $\boldsymbol{z}_{i-1}$ and negative along $-\boldsymbol{z}_{i-1}$. Thus, as an example, Figure 2.3(c) indicates a positive displacement, $d_2 > 0$, and Figure 2.3(d) a negative displacement, $d_2 < 0$. Other dimensions, such as ℓ and m in Figures 2.3(c,d), are drawn with double arrowheads, as in standard drawing dimensioning (cotagem), and are always assumed positive in the context of the drawing. Thus allowing to express $d_2 = \ell$ and $d_2 = -m$, in the respective Figures.

Regarding changes in the joint coordinates, it is also noted that according to the D-H convention, a joint coordinate is zero when $d_i = 0$ or $\vartheta_i = 0$. However, in practice, it may

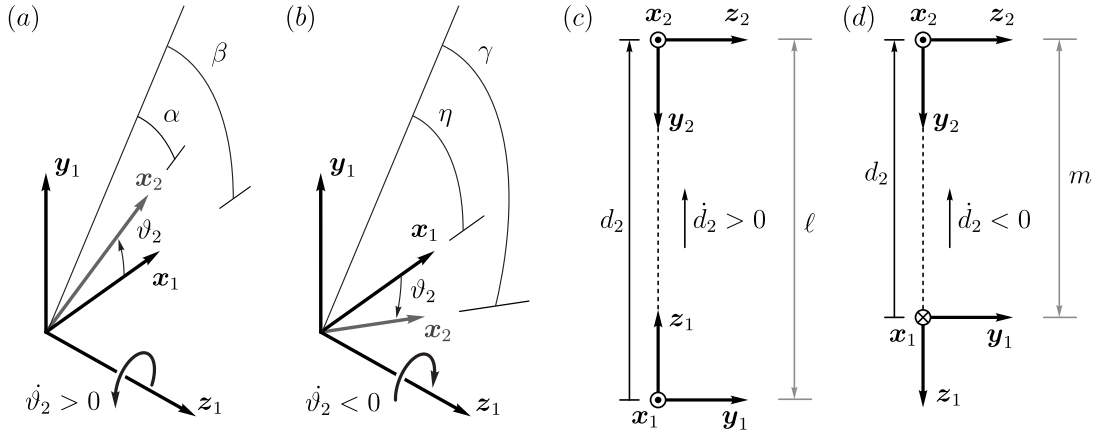

Figure 2.3: Angle and distance nomenclature. (a) Positive and (b) negative joint rotations. (c) Positive and (d) negative joint displacements.

be desirable to redefine the zero of the joint coordinate in a way that associates this value with a specific configuration of the robot arm, such as in a home position. In these cases, it is straightforward to introduce the necessary offsets in (2.2) by letting $d_i = d_i' +$ offset or $\vartheta_i = \vartheta_i' +$ offset, where d_i' or ϑ_i' become the new joint coordinate.

On a final note, for the sake of not overloading the drawings, it will be usual to not draw all of the axes in a frame. Thus, it is recalled that all illustrated frames are right-handed orthonormal frames.

3 Circular manipulator

Consider the circular manipulator illustrated in Figure 3.1. Its reference frames have been placed, at each link, in Figure 3.2, resulting in the Denavit-Hartenberg parameters gathered in Table 3.1.

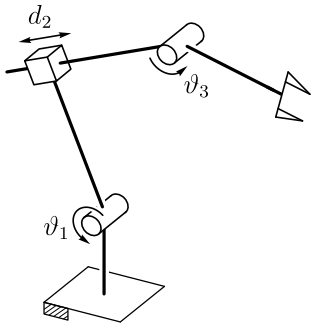

Figure 3.1: Circular manipulator.

To solve the inverse kinematics, consider the known end-effector's desired position as

$$\boldsymbol{p}_e = \left(\boldsymbol{r}^o_{o,3}\right)_d = \begin{pmatrix} e_x & e_y & 0 \end{pmatrix}^\intercal . \tag{3.1}$$

Since the manipulator is planar, the desired orientation may be written from its angle of rotation, termed ϕ_d, such that it corresponds to a rotation about $\boldsymbol{z}_o$,

$$(\boldsymbol{R}^o_3)_d = \begin{pmatrix} \boldsymbol{x}^o_3 & \boldsymbol{y}^o_3 & \boldsymbol{z}^o_3 \end{pmatrix}_d = \boldsymbol{R}_z(\phi_d) = \begin{pmatrix} \mathrm{c}_{\phi_d} & -\mathrm{s}_{\phi_d} & 0 \\ \mathrm{s}_{\phi_d} & \mathrm{c}_{\phi_d} & 0 \\ 0 & 0 & 1 \end{pmatrix} . \tag{3.2}$$

The kinematics can now be decoupled to determine the desired position for the origin of frame two, termed the wrist. Its position may be written as

$$\boldsymbol{p}_w = \begin{pmatrix} w_x & w_y & 0 \end{pmatrix}^\intercal = \left(\boldsymbol{r}^o_{o,3}\right)_d - a_3 \left(\boldsymbol{x}^o_3\right)_d . \tag{3.3}$$

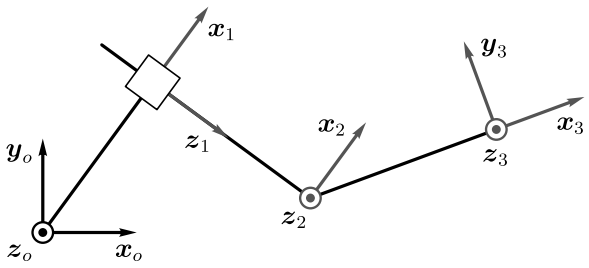

Figure 3.2: Circular manipulator's reference frames corresponding to Table 3.1.

Table 3.1: D-H parameters

i	d_i	ϑ_i	a_i	α_i
1	0	ϑ_1	a_1	$\pi/2$
2	d_2	0	0	$-\pi/2$
3	0	ϑ_3	a_3	0

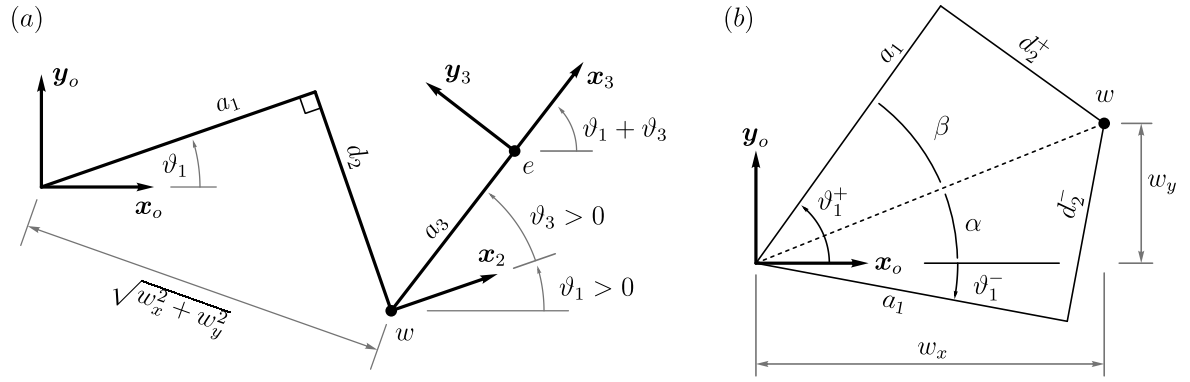

Figure 3.3: Relevant geometry for determining the configuration of (a) the second joint and (b) the first joint.

In this fashion, the coordinates of the wrist, $w_x = e_x - a_3\,\cos(\phi_d)$ and $w_y = e_y - a_3\,\sin(\phi_d)$, are also known quantities. Thus, the configuration of joints one and two can be solved from the position of point w. Moreover, independently of ϑ_1, the distance of w to the origin, $\|\boldsymbol{p}_w\| = \sqrt{w_x^2 + w_y^2}$, varies only as a function of the joint coordinate d_2, as can be gathered from Figure 3.3(a). Therefore, it is also true from $\|\boldsymbol{p}_w\|{=}\sqrt{a_1^2 + d_2^2}$ that the following holds,

$$d_2^{\pm} = \pm\sqrt{w_x^2 + w_y^2 - a_1^2}\,, \tag{3.4}$$

denoting two solutions for the prismatic joint. One solution is positive, $d_2^+ > 0$, and the other one is negative, $d_2^- < 0$. Both solutions are illustrated in Figure 3.3(b), from which two corresponding solutions follow for ϑ_1. To write these solutions define angles α and β as illustrated,

$$\alpha = \arctan(w_y, w_x) \quad , \quad \beta = \arctan(d_2^+, a_1)\,, \tag{3.5}$$

to conclude that

$$\vartheta_1^+ = \alpha + \beta \quad , \quad \vartheta_1^- = \alpha - \beta\,. \tag{3.6}$$

Finally, note that $\phi_d = \vartheta_1 + \vartheta_3$, to write the two sets of solutions gathered in Table 3.2.

Table 3.2: Circular manipulator's solutions, as in (3.2), (3.4) and (3.6).

$$\text{I:}\begin{cases}\vartheta_1 = \alpha + \beta\\ d_2 = \sqrt{w_x^2 + w_y^2 - a_1^2}\\ \vartheta_3 = \phi_d - (\alpha + \beta)\end{cases} \qquad \text{II:}\begin{cases}\vartheta_1 = \alpha - \beta\\ d_2 = -\sqrt{w_x^2 + w_y^2 - a_1^2}\\ \vartheta_3 = \phi_d - (\alpha - \beta)\end{cases}$$

4 Stadium manipulator

Consider the stadium manipulator illustrated in Figure 4.1. Its reference frames have been placed, at each link, in Figure 4.2, resulting in the Denavit-Hartenberg parameters gathered in Table 4.1.

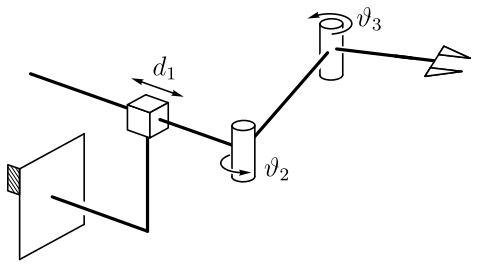

Figure 4.1: Stadium manipulator.

To solve its inverse kinematics, consider the known end-effector's desired position as

$$\boldsymbol{p}_e = \left(\boldsymbol{r}^o_{o,3}\right)_d = \begin{pmatrix} e_x & 0 & e_z \end{pmatrix}^\intercal . \tag{4.1}$$

Since the manipulator is planar, the desired end-effector orientation may be defined from its angle of rotation, ϕ_d, about $-\boldsymbol{y}_o$, such that

$$(\boldsymbol{R}^o_3)_d = \begin{pmatrix} \boldsymbol{x}^o_3 & \boldsymbol{y}^o_3 & \boldsymbol{z}^o_3 \end{pmatrix}_d = \boldsymbol{R}_y(-\phi_d)\,\boldsymbol{R}_x\!\left(\frac{\pi}{2}\right) = \begin{pmatrix} \mathrm{c}_{\phi_d} & -\mathrm{s}_{\phi_d} & 0 \\ 0 & 0 & -1 \\ \mathrm{s}_{\phi_d} & \mathrm{c}_{\phi_d} & 0 \end{pmatrix} . \tag{4.2}$$

The kinematics can now be decoupled between the end-effector and the wrist, as in Figure 4.3(a), to determine a desired position for the origin of frame two, termed $\boldsymbol{p}_w = \left(\boldsymbol{r}^o_{o,2}\right)_d$, through

$$\boldsymbol{p}_w = \begin{pmatrix} w_x & 0 & w_z \end{pmatrix}^\intercal = \left(\boldsymbol{r}^o_{o,3}\right)_d - a_3\,(\boldsymbol{x}^o_3)_d \ , \tag{4.3}$$

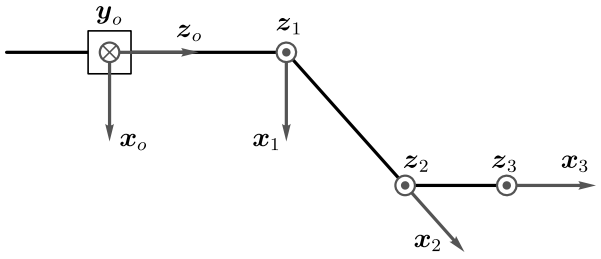

Figure 4.2: Stadium manipulator's reference frames corresponding to Table 4.1.

Table 4.1: D-H parameters

i	d_i	ϑ_i	a_i	α_i
1	d_1	0	0	$\pi/2$
2	0	ϑ_2	a_2	0
3	0	ϑ_3	a_3	0

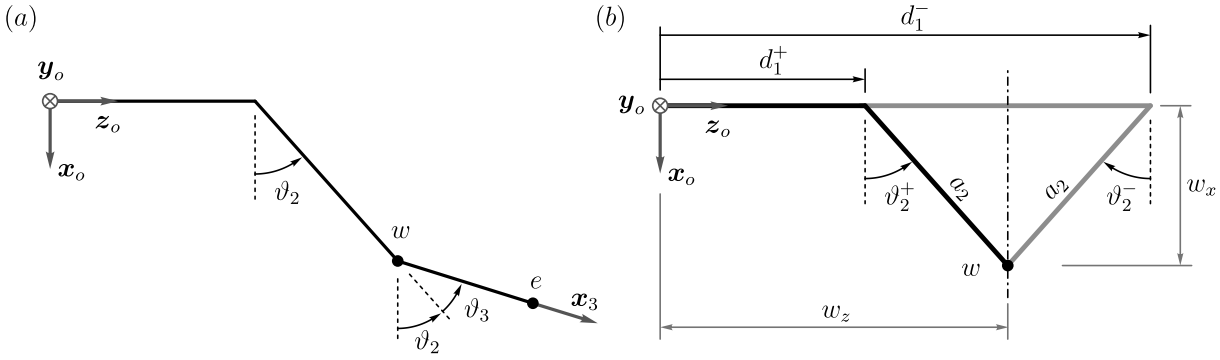

Figure 4.3: (a) Kinematic decoupling between points e and w. (b) Solution for the first two joints, as a function of the coordinates of point w.

resulting in $w_x = e_x - a_3\,\cos(\phi_d)$ and $w_z = e_z - a_3\,\sin(\phi_d)$.

Then, from Figure 4.3(b), it is clear that there are two solutions for the manipulator's inverse kinematics, best understood from the symmetry between ϑ_2^- and ϑ_2^+. Thus,

$$\vartheta_2^+ = \arccos\left(\frac{w_x}{a_2}\right) \quad , \quad \vartheta_2^- = -\arccos\left(\frac{w_x}{a_2}\right) , \tag{4.4}$$

and two solutions follows for d_1, as

$$d_1^+ = w_z - a_2\,\sin\left(\vartheta_2^+\right) \quad , \quad d_1^- = w_z + a_2\,\sin\left(\vartheta_2^+\right) . \tag{4.5}$$

Finally, noting that $\phi_d = \vartheta_2 + \vartheta_3$, the two sets of solutions can now be gathered in Table 4.2.

Table 4.2: Stadium manipulator's solutions, as in (4.2), (4.4) and (4.5).

$$\text{I:} \begin{cases} d_1 = d_1^+ \\ \vartheta_2 = \vartheta_2^+ \\ \vartheta_3 = \phi_d - \vartheta_2^+ \end{cases} \qquad \text{II:} \begin{cases} d_1 = d_1^+ + 2\,a_2\,\sin\left(\vartheta_2^+\right) \\ \vartheta_2 = -\vartheta_2^+ \\ \vartheta_3 = \phi_d + \vartheta_2^+ \end{cases}$$

5 SCARA manipulator

Consider now the SCARA (Selective Compliance Assembly Robotic Arm) manipulator illustrated in Figure 5.1, whose reference frames have been drawn, resulting in the D-H parameters in Table 5.1. The solution for its first two joints is the same as for the two-link planar arm, whose analytical solution can be found in [3]. A geometric solution for its inverse kinematics can also be found in [5].

Let then the desired position and orientation for the end-effector be defined as

$$\left(\boldsymbol{r}_{o,4}^{o}\right)_d = \begin{pmatrix} e_x & e_y & e_z \end{pmatrix}^{\mathsf{T}} \;,\; \left(\boldsymbol{R}_4^o\right)_d = \begin{pmatrix} \boldsymbol{x}_4^o & \boldsymbol{y}_4^o & \boldsymbol{z}_4^o \end{pmatrix}_d = \begin{pmatrix} \mathrm{c}_{\phi_d} & -\mathrm{s}_{\phi_d} & 0 \\ \mathrm{s}_{\phi_d} & \mathrm{c}_{\phi_d} & 0 \\ 0 & 0 & 1 \end{pmatrix} . \quad (5.1)$$

For the chosen D-H parameterization, the third joint (prismatic) can be immediately solved as $d_3 = e_z$. Now, since the x and y coordinates of the end-effector's position are the same as those of frame two, the solutions for the first two joints can be obtained from a planar arm projection, as in Figure 5.2(a). Thus, as illustrated, to see the two distinct solutions, draw two circles C_1 and C_2 with radii a_1 and a_2, centered at the origins of frame zero and frame two. The intersection of these circles yields then two solutions for the position of frame one, comprising the solutions of the manipulator. If there is no intersection then no solution exists.

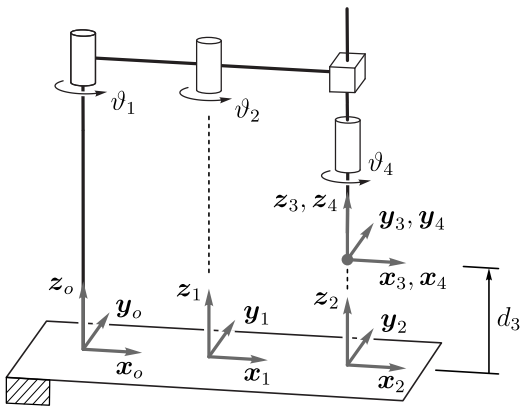

Figure 5.1: SCARA manipulator's reference frames corresponding to Table 5.1.

Table 5.1: D-H parameters

i	d_i	ϑ_i	a_i	α_i
1	0	ϑ_1	a_1	0
2	0	ϑ_2	a_2	0
3	d_3	0	0	0
4	0	ϑ_4	0	0

To determine the second joint's configuration, the law of cosines [6] is now derived with recourse to Figure 5.2(b), by noticing that $\|\boldsymbol{r}_{o,2}\|$ is only a function of ϑ_2. To this end, express the coordinates of this displacement in frame one, as

$$\boldsymbol{r}_{o,2}^{1} = \boldsymbol{r}_{o,1}^{1} + \boldsymbol{r}_{1,2}^{1} = \begin{pmatrix} a_1 \\ 0 \\ 0 \end{pmatrix} + \begin{pmatrix} a_2\,\mathrm{c}_2 \\ a_2\,\mathrm{s}_2 \\ 0 \end{pmatrix} = \begin{pmatrix} a_1 + a_2\,\mathrm{c}_2 \\ a_2\,\mathrm{s}_2 \\ 0 \end{pmatrix} , \quad (5.2)$$

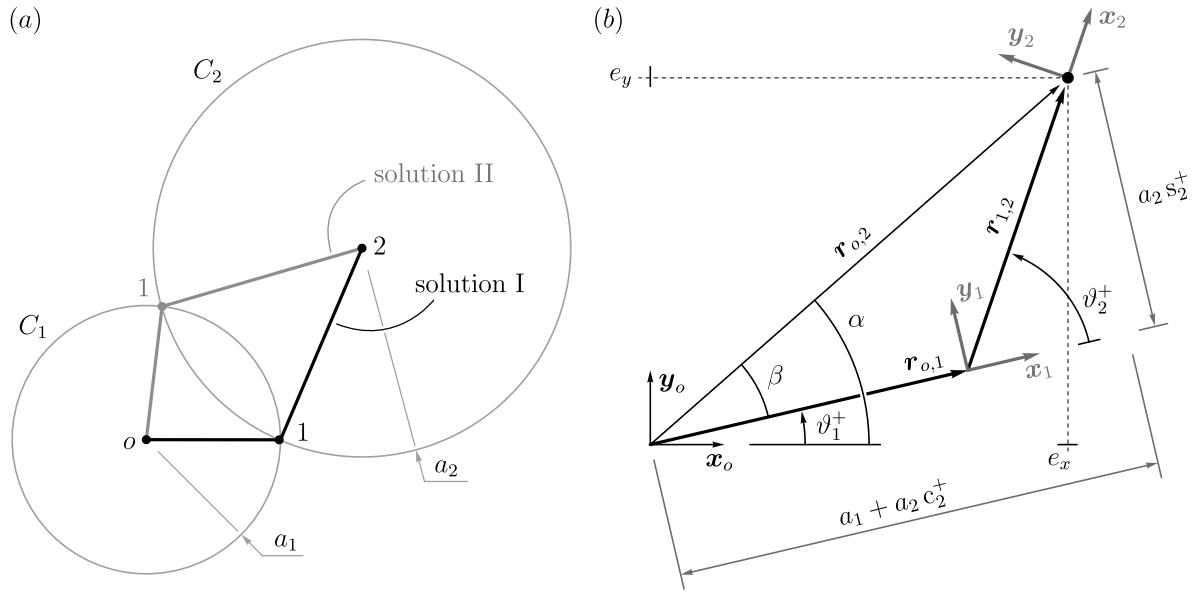

Figure 5.2: (a) Planar arm solutions. (b) Solution for the first two joints.

Equating the length with $\left\|(\boldsymbol{r}_{o,2})_d\right\| = \sqrt{e_x^2 + e_y^2}$ yields $e_x^2 + e_y^2 = (a_1 + a_2\,\mathrm{c}_2)^2 + (a_2\,\mathrm{s}_2)^2 = a_1^2 + a_2^2 + 2\,a_1\,a_2\,\mathrm{c}_2$, which can be solved for c_2 to find

$$\mathrm{c}_2 = \frac{e_x^2 + e_y^2 - a_1^2 - a_2^2}{2\,a_1\,a_2}\,. \tag{5.3}$$

Now, applying the Pythagorean identity, $\mathrm{c}_2^2 + \mathrm{s}_2^2 = 1$, the distinct solutions acknowledged in Figure 5.2(a) can be obtained by writing

$$\mathrm{s}_2^{\pm} = \pm\sqrt{1 - \mathrm{c}_2^2}\,, \tag{5.4}$$

resulting in the second joint's coordinate,

$$\vartheta_2^+ = \mathsf{arctan}\big(\mathrm{s}_2^+, c_2\big)\ , \quad \vartheta_2^- = \mathsf{arctan}\big(\mathrm{s}_2^-, c_2\big)\ . \tag{5.5}$$

The first joint can also be solved from the projection in Figure 5.2, by noting that

$$\alpha = \mathsf{arctan}(e_y, e_x)\ , \quad \beta = \mathsf{arctan}\big(a_2\,\mathrm{s}_2^+, a_1 + a_2\,\mathrm{c}_2\big)\ . \tag{5.6}$$

From this realization it is straightforward to write the two solutions for the first joint, as

$$\vartheta_1^+ = \alpha - \beta\,, \quad \vartheta_1^- = \alpha + \beta\,. \tag{5.7}$$

Finally, the fourth joint can be solved by noting that all axes of rotation in the SCARA manipulator are parallel. Therefore, the desired orientation angle of the end-effector, ϕ_d (5.1), must be the same as

$$\phi_d = \vartheta_1 + \vartheta_2 + \vartheta_4\,. \tag{5.8}$$

Table 5.2: SCARA manipulator's solutions, as in (5.1), (5.5) and (5.7).

$$\text{I:}\begin{cases}\vartheta_1 = \vartheta_1^+\\ \vartheta_2 = \vartheta_2^+\\ d_3 = e_z\\ \vartheta_4 = \phi_d - \vartheta_1^+ - \vartheta_2^+\end{cases} \qquad \text{II:}\begin{cases}\vartheta_1 = \vartheta_1^-\\ \vartheta_2 = \vartheta_2^-\\ d_3 = e_z\\ \vartheta_4 = \phi_d - \vartheta_1^- - \vartheta_2^-\end{cases}$$

The described solutions are now gathered in Table 5.2.

6 Piston-rod-crank system

Consider now the piston, rod and crank system illustrated in Figure 6.1. Its frames are placed according to the D-H convention and the corresponding parameters are given in Table 6.1. Note that when this system is meant to represent its namesake, then link one represents the crankshaft, link two the connection rod and link three the piston. In which case, link four would represent an unmoving element (the cylinder) meant to define the piston's translation axis.

Since the mechanism is planar, it is at most possible to ascribe two coordinates for the position of link four and another one for its orientation. Thus, three degrees of freedom of the mechanism can be constrained and since it has a total of four degrees of freedom then there must be one degree of freedom that is not subject to the previous Cartesian constraints. In other words, the mechanism is redundant.

In general, the redundant degree of freedom of a mechanism can be a joint coordinate or a combination of joint coordinates. In this simple example the redundancy will be associated with a single joint coordinate. Thus, in §6.1 the redundancy will be associated with the displacement of the piston and in §6.2 with the rotation of the crankshaft.

6.1 Piston spanning

For the first case, as illustrated in Figure 6.2(a), there is a line L_1 collinear with the constraint $(\boldsymbol{z}_4)_d$ along which the origin of frame three (point w) can be placed, such that the intersection between circles C_1 and C_2 returns a solution, much like in §5. The solution for this case is now described, as follows.

Let then the desired position for reference frame four be defined as

$$\left(\boldsymbol{r}^o_{o,4}\right)_d = \begin{pmatrix} e_x & e_y & 0 \end{pmatrix}^\mathsf{T}, \tag{6.1}$$

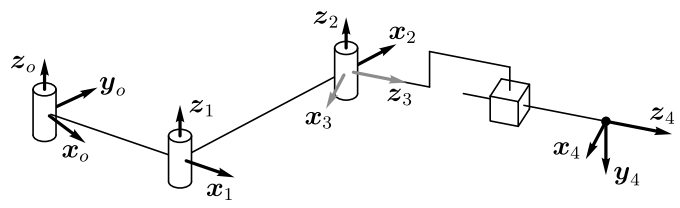

Figure 6.1: Piston-Rod-Crank system's reference frames corresponding to Table 6.1.

Table 6.1: D-H parameters

i	d_i	ϑ_i	a_i	α_i
1	0	ϑ_1	a_1	0
2	0	ϑ_2	a_2	0
3	0	ϑ_3	0	$-\pi/2$
4	d_4	0	0	0

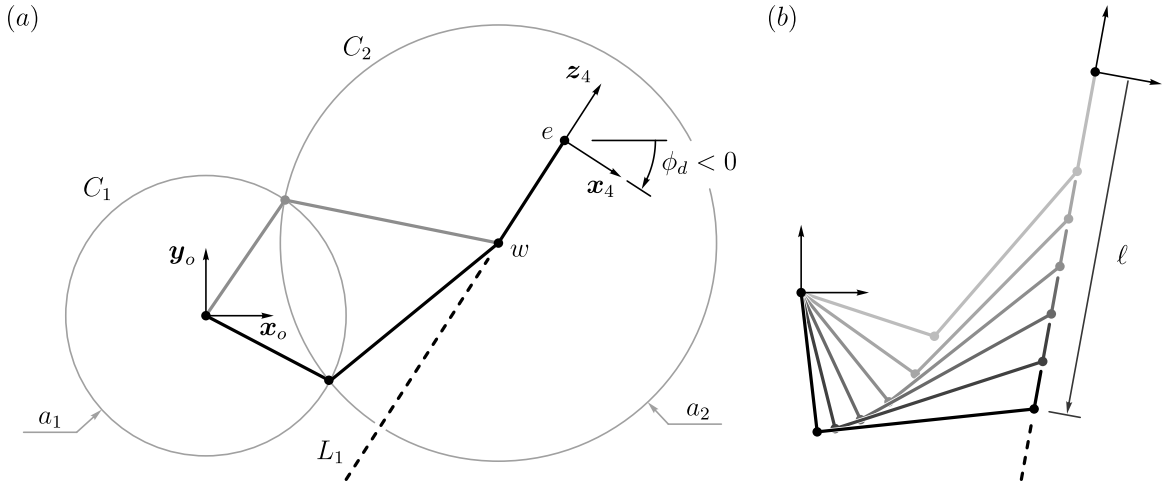

Figure 6.2: Piston-rod-crank system. (a) Discrete solutions arising from the placement of point w. (b) Nullspace motion arising from the piston's displacement (fourth joint).

and the desired orientation be assigned by an angle ϕ_d, such that

$$(\boldsymbol{R}_4^o)_d = \begin{pmatrix} \boldsymbol{x}_4^o & \boldsymbol{y}_4^o & \boldsymbol{z}_4^o \end{pmatrix}_d = \boldsymbol{R}_z(\phi_d)\,\boldsymbol{R}_x(-\pi/2) = \begin{pmatrix} \mathrm{c}_{\phi_d} & 0 & -\mathrm{s}_{\phi_d} \\ \mathrm{s}_{\phi_d} & 0 & \mathrm{c}_{\phi_d} \\ 0 & -1 & 0 \end{pmatrix} . \tag{6.2}$$

As illustrated in Figure 6.2(b), define also the coordinate ℓ meant to span the system's space of solutions (or nullspace motions). The system's configuration is then defined by the set of coordinates (e_x, e_y, ϕ_d, ℓ). Decoupling can now be applied to define the origin of frame three through

$$\boldsymbol{p}_w = \begin{pmatrix} w_x & w_y & 0 \end{pmatrix}^{\mathsf{T}} \triangleq \big(\boldsymbol{r}_{o,3}^o\big)_d = \big(\boldsymbol{r}_{o,4}^o\big)_d - \ell\,(\boldsymbol{z}_4^o)_d \;, \tag{6.3}$$

and the solution for the first two joints comprises the solution for the two-link planar arm, as in the SCARA manipulator (§5).

Thus, following the illustration in Figure 6.3(I), employ the law of cosines as derived in (5.3), to note that $w_x^2 + w_y^2 = a_1^2 + a_2^2 + 2\,a_1\,a_2\,\mathrm{c}_2$. Thus,

$$\mathrm{c}_2 = \frac{w_x^2 + w_y^2 - a_1^2 - a_2^2}{2\,a_1\,a_2} \quad , \quad \mathrm{s}_2^{\pm} = \pm\sqrt{1 - \mathrm{c}_2^2}\,, \tag{6.4}$$

where two solutions have been gathered, one with positive s_2 (Figure 6.3,I) and another one with negative s_2 (Figure 6.3,II). From this result, the solutions for the second joint become

$$\vartheta_2^+ = \mathsf{arctan}\big(\mathrm{s}_2^+, \mathrm{c}_2\big) \;, \quad \vartheta_2^- = \mathsf{arctan}\big(\mathrm{s}_2^-, \mathrm{c}_2\big) \;. \tag{6.5}$$

Gathering now the auxiliary angles

$$\alpha = \mathsf{arctan}(w_y, w_x) \;, \quad \beta = \mathsf{arctan}\big(a_2\,\mathrm{s}_2^+, a_1 + a_2\,\mathrm{c}_2\big) \;, \tag{6.6}$$

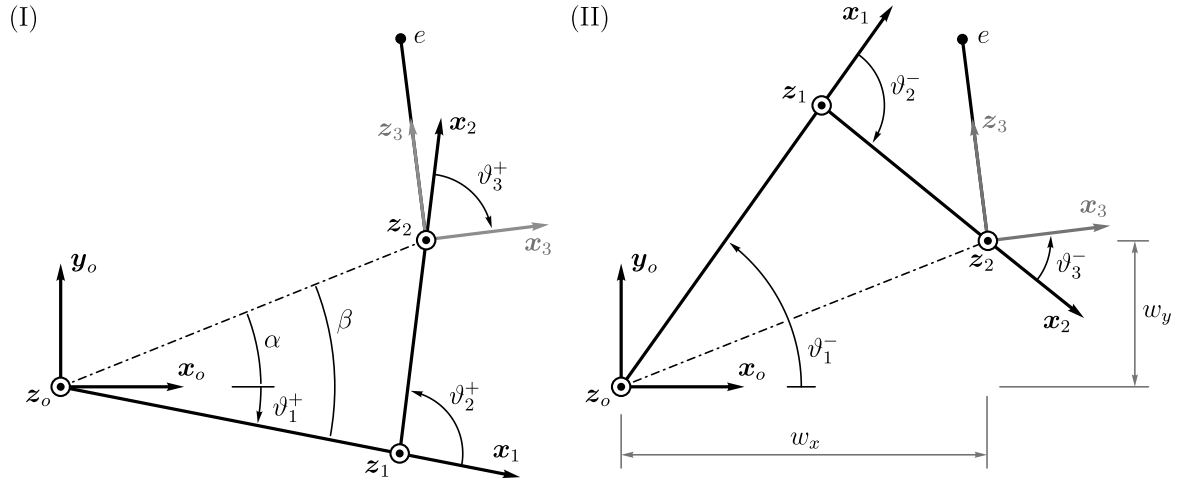

Figure 6.3: Piston-Rod-Crank system's solutions, for a given piston displacement.

Table 6.2: Piston-rod-crank system's solutions, as in (6.5), (6.7) and (6.8).

$$\text{I:} \begin{cases} \vartheta_1 = \vartheta_1^+ \\ \vartheta_2 = \vartheta_2^+ \\ \vartheta_3 = \vartheta_3^+ \\ d_4 = \ell \end{cases} \qquad \text{II:} \begin{cases} \vartheta_1 = \vartheta_1^- \\ \vartheta_2 = \vartheta_2^- \\ \vartheta_3 = \vartheta_3^- \\ d_4 = \ell \end{cases}$$

the solutions for the first joint can be written as

$$\vartheta_1^+ = \alpha - \beta \quad , \quad \vartheta_1^- = \alpha + \beta \, . \tag{6.7}$$

Now, noting that $\phi_d = \vartheta_1 + \vartheta_2 + \vartheta_3$, then it is true that

$$\vartheta_3^+ = \phi_d - \vartheta_1^+ - \vartheta_2^+ \quad , \quad \vartheta_3^- = \phi_d - \vartheta_1^- - \vartheta_2^- \, . \tag{6.8}$$

The system has two distinct (discrete) solutions, gathered in Table 6.2, along which there are infinite (continuous) solutions, spanned through coordinate ℓ.

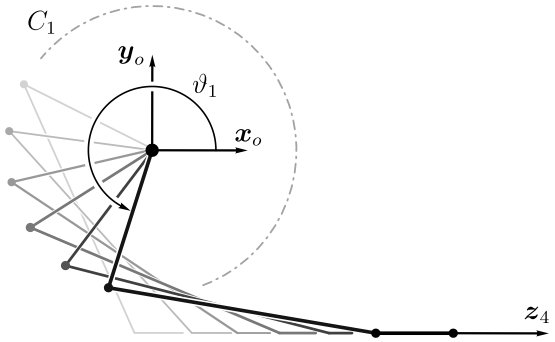

Figure 6.4: Nullspace motion arising from the crankshaft's rotation (first joint).

6.2 Crankshaft spanning

An alternate solution arises if the crankshaft's rotation is chosen as the degree of freedom which spans the system's nullspace. As illustrated in Figure 6.4, this coordinate corresponds indeed to the first joint, ϑ_1. Echoing now the definitions in (6.1) and (6.2), note in Figure 6.5(a) that the origin of frame one can now be placed anywhere along circle C_1, with coordinates that are fixed as a function of ϑ_1. Thus, define

$$\left(\boldsymbol{r}^o_{1,4}\right)_d = \begin{pmatrix} e_x - a_1\,\mathrm{c}_1 \\ e_y - a_1\,\mathrm{s}_1 \\ 0 \end{pmatrix} . \tag{6.9}$$

From this realization, it is true that the coordinates of joints two, three and four are fixed as a function of the former definitions, and a solution may be obtained as follows.

Consider now expressing the vector from the origin of frame one to the origin of frame four, with coordinate expressed in the last frame, through

$$\left(\boldsymbol{r}^4_{1,4}\right)_d = \left(\boldsymbol{R}^o_4\right)^{\mathsf{T}}_d \left(\boldsymbol{r}^o_{1,4}\right)_d \triangleq \begin{pmatrix} s_x \\ 0 \\ s_z \end{pmatrix} . \tag{6.10}$$

Then the coordinates s_x and s_z are also known quantities, which can now be employed, through Figure 6.5(b), to determine the system's configuration. This solution is now very similar to the one in §4. To determine the fourth joint, employ the Pythagorean theorem to write

$$d_4^- = s_z - \sqrt{a_2^2 - s_x^2} \quad , \quad d_4^+ = s_z + \sqrt{a_2^2 - s_x^2}\,. \tag{6.11}$$

Now, for the third joint's solutions, employ the inverse tangent function to write

$$\vartheta_3^- = -\arctan\!\left(s_z - d_4^-, s_x\right) \quad , \quad \vartheta_3^+ = \arctan\!\left(s_z - d_4^-, s_x\right) . \tag{6.12}$$

To determine the second joint, note that $\vartheta_1 + \vartheta_2 + \vartheta_3 = \phi_d$. Thus,

$$\vartheta_2^- = \phi_d - \vartheta_1 - \vartheta_3^- \quad , \quad \vartheta_2^+ = \phi_d - \vartheta_1 - \vartheta_3^+ . \tag{6.13}$$

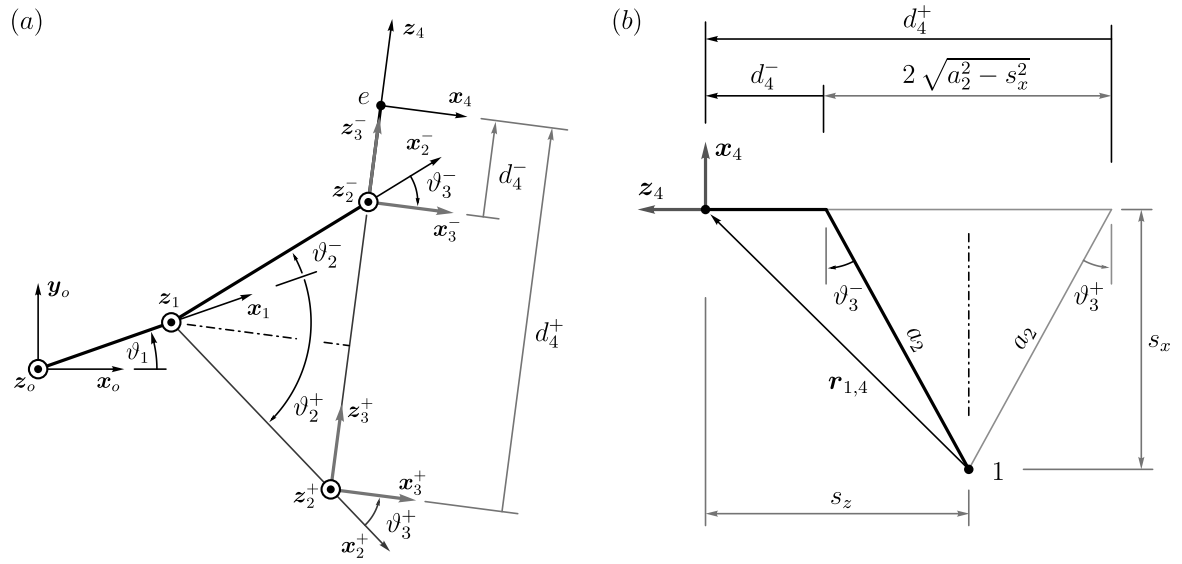

Figure 6.5: (a) Piston-Rod-Crank system's solutions, for a given crank angle ξ. (b) Kinematic decoupling.

Table 6.3: Piston-rod-crank system's solutions, as in (6.11-6.13).

$$\text{I:} \begin{cases} \vartheta_1 = \vartheta_1 \\ \vartheta_2 = \vartheta_2^- \\ \vartheta_3 = \vartheta_3^- \\ d_4 = d_4^- \end{cases} \qquad \text{II:} \begin{cases} \vartheta_1 = \vartheta_1 \\ \vartheta_2 = \vartheta_2^+ \\ \vartheta_3 = \vartheta_3^+ \\ d_4 = d_4^+ \end{cases}$$

The present solutions are finally gathered in Table 6.3, as a function of the crankshaft's rotation, ϑ_1.

7 Toroidal arm

Consider now the toroidal manipulator illustrated in Figure 7.1. Its frames are placed according to the D-H convention and the corresponding parameters are given in Table 7.1. Making its three degrees of freedom available to specify a Cartesian position, let then its desired position be defined as

$$\left(\boldsymbol{r}_{o,3}^{o}\right)_{d} = \begin{pmatrix} e_x & e_y & e_z \end{pmatrix}^{\intercal} . \tag{7.1}$$

In Figure 7.2, two solutions which satisfy this constraint are illustrated. The first notated as $\boldsymbol{q}^{\mathrm{I}} = (\vartheta_1^{\mathrm{I}}, \vartheta_2^{\mathrm{I}}, d_3^{\mathrm{I}})^{\intercal}$ and the second $\boldsymbol{q}^{\mathrm{II}} = (\vartheta_1^{\mathrm{II}}, \vartheta_2^{\mathrm{II}}, d_3^{\mathrm{II}})^{\intercal}$. The present manipulator topology is typical of industrial vehicles, being $\boldsymbol{q}^{\mathrm{I}}$ the typical configuration observed in excavators, for instance, and $\boldsymbol{q}^{\mathrm{II}}$ the typical configuration observed in hydraulic ladders, as in a fire fighting vehicle.

The previous solutions can thus be identified by a difference of π in the first joint angle. Moreover, following the illustration,

$$\vartheta_1^{\mathrm{I}} = \arctan(e_y, e_x) \ , \tag{7.2}$$

and the second solution for the first joint follows,

$$\vartheta_1^{\mathrm{II}} = \pi + \vartheta_1^{\mathrm{I}} . \tag{7.3}$$

To determine the second joint define the construction angles

$$\alpha = \arctan\Big(e_z, \sqrt{e_x^2 + e_y^2} - a_1\Big) \quad , \quad \beta = \arctan\Big(e_z, \sqrt{e_x^2 + e_y^2} + a_1\Big) \ . \tag{7.4}$$

Noting now that the value of ϑ_2^{I} is here illustrated as a negative joint angle, then

$$\vartheta_2^{\mathrm{I}} = -\left(\frac{\pi}{2} - \alpha\right) . \tag{7.5}$$

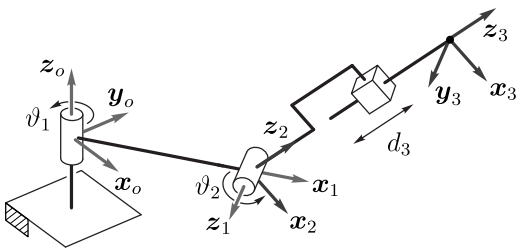

Figure 7.1: Toroidal manipulator's reference frames corresponding to Table 7.1.

Table 7.1: D-H parameters

i	d_i	ϑ_i	a_i	α_i
1	0	ϑ_1	a_1	$\pi/2$
2	0	ϑ_2	0	$-\pi/2$
3	d_3	0	0	0

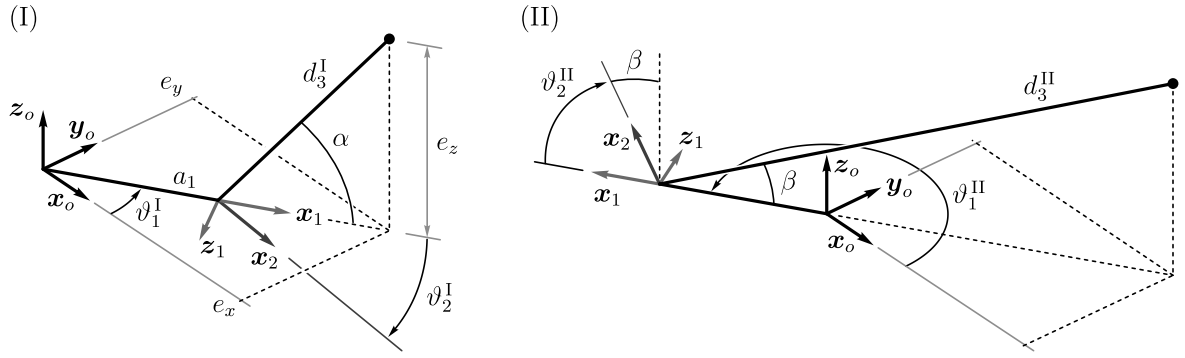

Figure 7.2: Toroidal manipulator's first and second solutions, out of four.

For its second solution, note that the value of $\vartheta_2^{\mathrm{II}}$ is positive in the illustration, to write

$$\vartheta_2^{\mathrm{II}} = \frac{\pi}{2} - \beta\,. \tag{7.6}$$

Finally, the solutions for the third joint's displacement follow from Pythagoras' theorem, to write the smallest length, d_3^{I}, and the largest, d_3^{II}, as

$$d_3^{\mathrm{I}} = \sqrt{\left(\sqrt{e_x^2+e_y^2} - a_1\right)^2 + e_z^2} \quad , \quad d_3^{\mathrm{II}} = \sqrt{\left(\sqrt{e_x^2+e_y^2} + a_1\right)^2 + e_z^2}\,. \tag{7.7}$$

Finally, note that a negative sign for the third joint's displacement can also be chosen (not illustrated), which can be achieved by an additional half-turn, of $\pm\pi$, about the second joint. That said, the four sets of solutions can now be gathered into Table 7.2.

Table 7.2: Toroidal manipulator's solutions, as in (7.2), (7.3) and (7.5-7.7).

$$\text{I:}\begin{cases}\vartheta_1 = \vartheta_1^{\mathrm{I}}\\ \vartheta_2 = \vartheta_2^{\mathrm{I}}\\ d_3 = d_3^{\mathrm{I}}\end{cases} \quad \text{II:}\begin{cases}\vartheta_1 = \vartheta_2^{\mathrm{II}}\\ \vartheta_2 = \vartheta_2^{\mathrm{II}}\\ d_3 = d_3^{\mathrm{II}}\end{cases} \quad \text{III:}\begin{cases}\vartheta_1 = \vartheta_1^{\mathrm{I}}\\ \vartheta_2 = \vartheta_2^{\mathrm{I}} + \pi\\ d_3 = -d_3^{\mathrm{I}}\end{cases} \quad \text{IV:}\begin{cases}\vartheta_1 = \vartheta_2^{\mathrm{II}}\\ \vartheta_2 = \vartheta_2^{\mathrm{II}} + \pi\\ d_3 = -d_3^{\mathrm{II}}\end{cases}$$

8 Spherical arm

Consider now the spherical manipulator illustrated in Figure 8.1. Its reference frames are placed according to the D-H convention and the corresponding parameters are gathered into Table 8.1.

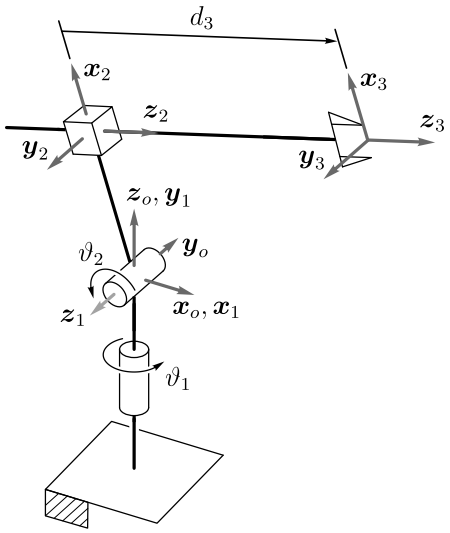

Figure 8.1: Spherical manipulator's reference frames corresponding to Table 8.1.

Table 8.1: D-H parameters

i	d_i	ϑ_i	a_i	α_i
1	0	ϑ_1	0	$\pi/2$
2	0	ϑ_2	a_2	$\pi/2$
3	d_3	0	0	0

Making its three degrees of freedom available to specify a Cartesian position for the end-effector, then its desired position can be defined as

$$\left(\boldsymbol{r}^o_{o,3}\right)_d = \begin{pmatrix} e_x & e_y & e_z \end{pmatrix}^\mathsf{T} . \tag{8.1}$$

Noting now that the origin of frames one, two and three lie in the plane formed by axes $\boldsymbol{x}_1$ and $\boldsymbol{y}_1$, as illustrated in Figure 8.2, then a particular solution for the first joint is given by

$$\vartheta_1^* = \mathsf{arctan}(e_y, e_x) . \tag{8.2}$$

The third joint's displacement can be found from Figure 8.2(I) to be

$$d_3^\pm = \pm\sqrt{e_x^2 + e_y^2 + e_z^2 - a_2^2} . \tag{8.3}$$

Indeed, this displacement can be either a positive displacement, d_3^+, as in Figures 8.2(I,IV), or a negative displacement, d_3^-, as in Figures 8.2(II,III). Returning now to Figure 8.2(I), the inverse of the tangent function allows to define the construction angles

$$\alpha = \mathsf{arctan}\left(e_z, \sqrt{e_x^2 + e_y^2}\right) , \quad \beta = \mathsf{arctan}\left(d_3^+, a_2\right) . \tag{8.4}$$

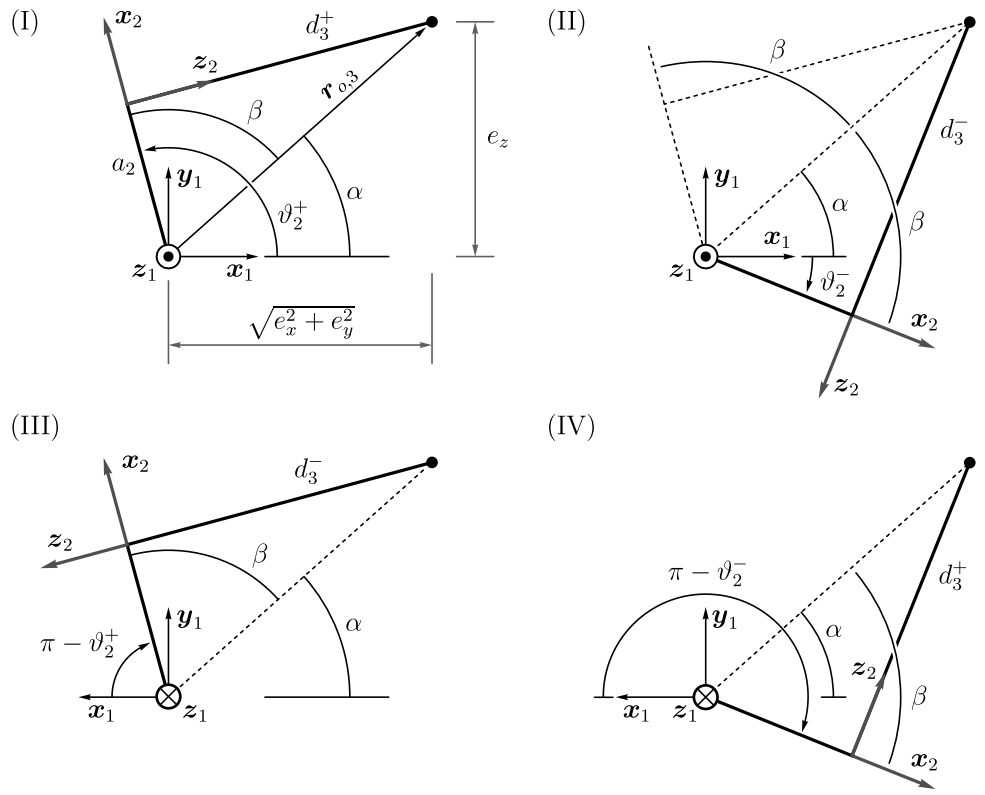

Figure 8.2: Spherical manipulator's solutions.

Thus, the second joint's configuration is determined through

$$\vartheta_2^+ = \alpha + \beta \quad , \quad \vartheta_2^- = \alpha - \beta \, . \tag{8.5}$$

Finally, note that the solutions illustrated in Figures 8.2(III,IV) require an additional half-turn of the first joint, of $\pm\pi$, to gather the set of solutions in Table 8.2.

Table 8.2: Spherical manipulator's solutions, as in (8.2-8.4).

$$\text{I:} \begin{cases} \vartheta_1 = \vartheta_1^* \\ \vartheta_2 = \alpha + \beta \\ d_3 = d_3^+ \end{cases} \quad \text{II:} \begin{cases} \vartheta_1 = \vartheta_1^* \\ \vartheta_2 = \alpha - \beta \\ d_3 = d_3^- \end{cases} \quad \text{III:} \begin{cases} \vartheta_1 = \vartheta_1^* + \pi \\ \vartheta_2 = \pi - \alpha - \beta \\ d_3 = d_3^- \end{cases} \quad \text{IV:} \begin{cases} \vartheta_1 = \vartheta_1^* + \pi \\ \vartheta_2 = \pi - \alpha + \beta \\ d_3 = d_3^+ \end{cases}$$

9 Stanford manipulator

Consider now the Stanford manipulator illustrated in Figure 9.1, whose reference frames have been placed in Figure 9.2, resulting in the D-H parameters gathered in Table 9.1. An algebraic solution for this manipulator's inverse kinematics can be found in [7].

The six degrees of freedom of the manipulator are available to specify a Cartesian position and orientation for the end-effector, whose desired value can be defined as

$$\left(\boldsymbol{r}_{o,6}^{o}\right)_d = \begin{pmatrix} e_x & e_y & e_z \end{pmatrix}^{\mathsf{T}} \quad , \quad \left(\boldsymbol{R}_6^o\right)_d = \begin{pmatrix} \boldsymbol{x}_6^o & \boldsymbol{y}_6^o & \boldsymbol{z}_6^o \end{pmatrix}_d . \tag{9.1}$$

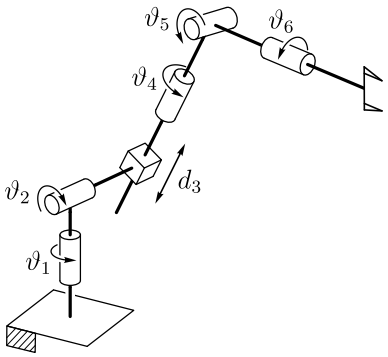

Figure 9.1: Stanford manipulator.

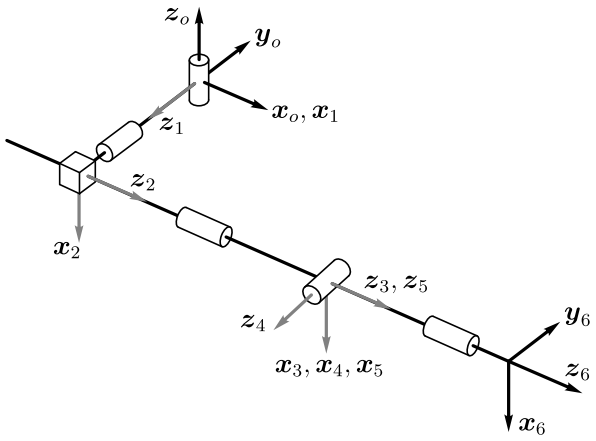

Figure 9.2: Stanford manipulator's reference frames corresponding to Table 9.1. The illustrated configuration is $\boldsymbol{q}^{\mathsf{T}} = (0, -\pi/2, d_3, 0, 0, 0)$ with $d_i > 0$.

Table 9.1: D-H parameters

i	d_i	ϑ_i	a_i	α_i
1	0	ϑ_1	0	$\pi/2$
2	d_2	ϑ_2	0	$-\pi/2$
3	d_3	0	0	0
4	0	ϑ_4	0	$\pi/2$
5	0	ϑ_5	0	$-\pi/2$
6	d_6	ϑ_6	0	0

Since the manipulator has a spherical wrist, its kinematic decoupling allows to split the inverse kinematics problem into the solution of the lower arm, comprising the first three joints,

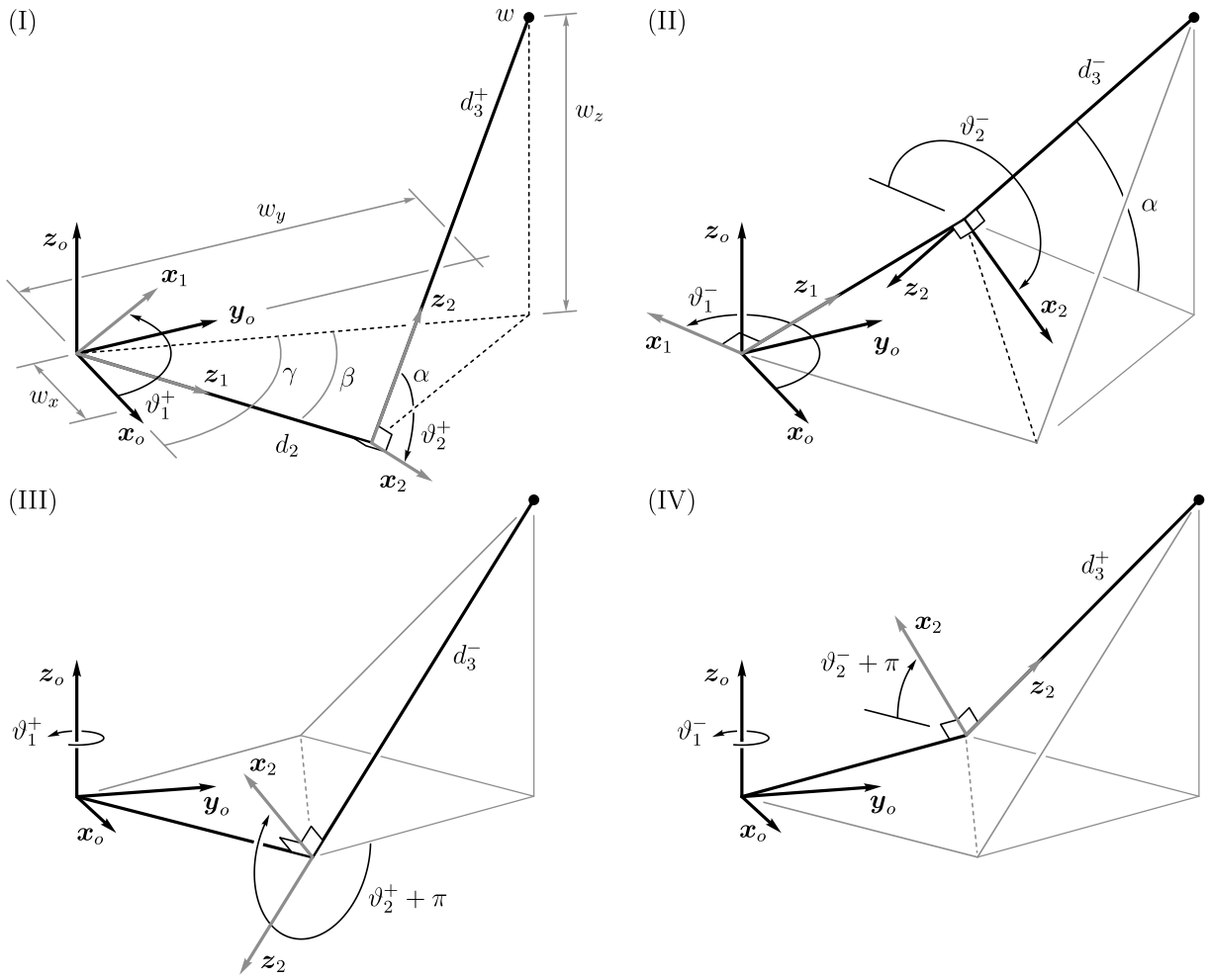

Figure 9.3: Stanford manipulator's solutions for the first three joints.

and the solution of the wrist, comprising the last three joints. Thus, from knowledge of the end-effector's desired position and orientation, the desired wrist position follows, at the origin of frame three,

$$\boldsymbol{p}_w = \begin{pmatrix} w_x & w_y & 0 \end{pmatrix}^{\mathsf{T}} \triangleq \left(\boldsymbol{r}_{o,3}^{o}\right)_d = \left(\boldsymbol{r}_{o,6}^{o}\right)_d - d_6 \left(\boldsymbol{z}_6^{o}\right)_d \,. \tag{9.2}$$

This position is determined from the configuration of the first three joints, whose solution is now given.

As illustrated in Figure 9.3, there are four solutions which satisfy the specified wrist's position. From this constraint, a solution for the third joint's displacement can be inspected from the right triangle formed by the origin of frames one, two and three (the wrist). Thus, from Pythagoras' theorem, it is true that $w_x^2{+}w_y^2{+}w_z^2{=}d_2^2{+}d_3^2$, and a pair of solutions can be found,

$$d_3^{\pm} = \pm\sqrt{w_x^2 + w_y^2 + w_z^2 - d_2^2}\,, \tag{9.3}$$

one where d_3^+ is positive, as in Figures 9.3(I,IV), and another where d_3^- is negative, as in

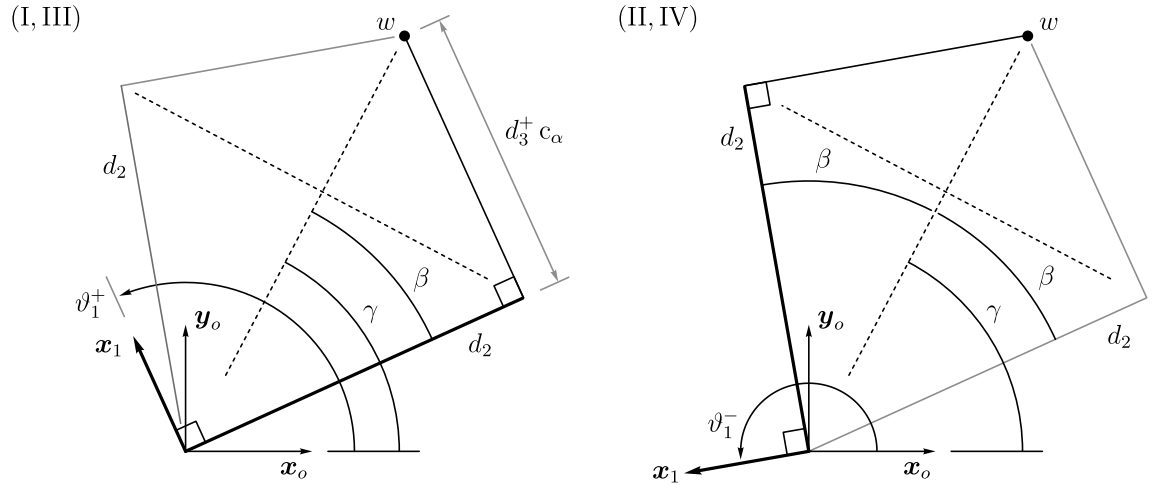

Figure 9.4: Lower arm projection onto plane $\langle \boldsymbol{x}, \boldsymbol{y} \rangle_o$.

Figures 9.3(II,III).

The next step is to determine joint two, which can be done from knowledge of angle α, in Figures 9.3(I,II). Thus, since $d_3^+ \, \sin(\alpha) = w_z$ and $\cos(\alpha) = \pm\sqrt{1 - \sin(\alpha)^2}$, it is true that

$$\alpha = \arctan\left(\frac{w_z}{d_3^+}, \sqrt{1 - \left(\frac{w_z}{d_3^+} \right)^2} \right) \; . \tag{9.4}$$

Finally, noting that the value of ϑ_2^+ was illustrated as a negative joint angle, its solution can now be written as

$$\vartheta_2^+ = -\left(\frac{\pi}{2} - \alpha \right) \; . \tag{9.5}$$

The solution can be now carried to the first joint, for which the construction angles β and γ have been illustrated in Figure 9.4, in the plane formed by $\boldsymbol{x}_o$ and $\boldsymbol{y}_o$. These construction angles can be calculated as

$$\beta = \arctan\big(d_3^+ \, \mathrm{c}_\alpha, d_2\big) \quad , \quad \gamma = \arctan(w_y, w_x) \; . \tag{9.6}$$

From this realization, a solution for the first joint's coordinate follows,

$$\vartheta_1^+ = \gamma - \beta + \frac{\pi}{2} \, . \tag{9.7}$$

The remaining solutions are analogous. From Figure 9.3(II) one finds the second joint's coordinate to be $\vartheta_2^- = \pi + (\pi/2 - \alpha)$, or

$$\vartheta_2^- = \frac{3\pi}{2} - \alpha \, , \tag{9.8}$$

and from Figure 9.4, the first joint follows as

$$\vartheta_1^- = \gamma + \beta + \frac{\pi}{2} \, . \tag{9.9}$$

The solutions in Figures 9.3(III,IV) follow from the previous ones, differing in the sign of the third joint's displacement, which can be achieved by an additional half-turn, of $\pm\pi$, about the second joint.

Having determined the configuration for the first three joints, both the desired orientation of the end-effector, $(\boldsymbol{R}_6^o)_d$, and the orientation of frame three, $(\boldsymbol{R}_3^o)_d$, are known quantities. Thus, from Table 9.1, and equation (2.2), the rotation between frames six and three can be expressed both symbolically and numerically, as

$$\boldsymbol{R}_o^3\,\boldsymbol{R}_6^o = \begin{pmatrix} \mathrm{c}_4\,\mathrm{c}_5\,\mathrm{c}_6 - \mathrm{s}_4\,\mathrm{s}_6 & -\mathrm{s}_4\,\mathrm{c}_6 - \mathrm{c}_4\,\mathrm{c}_5\,\mathrm{s}_6 & -\mathrm{c}_4\,\mathrm{s}_5 \\ \mathrm{s}_4\,\mathrm{c}_5\,\mathrm{c}_6 + \mathrm{c}_4\,\mathrm{s}_6 & \mathrm{c}_4\,\mathrm{c}_6 - \mathrm{s}_4\,\mathrm{c}_5\,\mathrm{s}_6 & -\mathrm{s}_4\,\mathrm{s}_5 \\ \mathrm{s}_5\,\mathrm{c}_6 & -\mathrm{s}_5\,\mathrm{s}_6 & \mathrm{c}_5 \end{pmatrix} \triangleq \begin{pmatrix} r_{11} & r_{12} & r_{13} \\ r_{21} & r_{22} & r_{23} \\ r_{31} & r_{32} & r_{33} \end{pmatrix} = \left(\boldsymbol{R}_6^3\right)_d\,, \tag{9.10}$$

where $\left(\boldsymbol{R}_6^3\right)_d$ is also a known quantity. The solution for ϑ_4, ϑ_5 and ϑ_6 is entirely analogous to the inverse problem in determining an Euler angles set [3, §2.4], which is now followed analytically. To do so, two different solutions are first acknowledged by noting that $r_{31}^2 + r_{32}^2 = \mathrm{s}_5^2$. Thus, the sine of ϑ_5 is free to change signs (or, ϑ_5 is free to change quadrants), through

$$\mathrm{s}_5^{\pm} = \pm\sqrt{r_{31}^2 + r_{32}^2}\,. \tag{9.11}$$

Let then s_5 be a positive quantity, $\mathrm{s}_5 \equiv \mathrm{s}_5^+$, then

$$\begin{cases} \vartheta_4^+ = \arctan(-r_{23}, -r_{13}) \\ \vartheta_5^+ = \arctan\left(\sqrt{r_{31}^2 + r_{32}^2}, r_{33}\right) \\ \vartheta_6^+ = \arctan(-r_{32}, r_{31}) \end{cases} \tag{9.12}$$

Alternatively, let s_5 be a negative quantity, $\mathrm{s}_5 \equiv -\mathrm{s}_5^+$, then

$$\begin{cases} \vartheta_4^- = \arctan(r_{23}, r_{23}) \\ \vartheta_5^- = \arctan\left(-\sqrt{r_{31}^2 + r_{32}^2}, r_{33}\right) \\ \vartheta_6^- = \arctan(r_{32}, -r_{31}) \end{cases} \tag{9.13}$$

Note also that, since $\arctan(y,x) = \arctan(-y,-x) + \pi$ and $\arctan(y,x) = -\arctan(-y,x)$, it is equally true that $\vartheta_4^- = \vartheta_4^+ + \pi$, $\vartheta_5^- = -\vartheta_5^+$ and $\vartheta_6^- = \vartheta_6^+ + \pi$.

The solutions have now been determined. Four sets of solutions of the lower arm (first three joints) and two sets of solutions for the spherical wrist (last three joints). Thus, the Stanford manipulator has eight distinct solutions, which are finally gathered in Table 9.2.

Table 9.2: Stanford manipulator's solutions, as in (9.3), (9.5), (9.7-9.9), (9.12) and (9.13).

$$\text{I:}\begin{cases}\vartheta_1 = \vartheta_1^+\\ \vartheta_2 = \vartheta_2^+\\ d_3 = d_3^+\\ \vartheta_4 = \vartheta_4^+\\ \vartheta_5 = \vartheta_5^+\\ \vartheta_6 = \vartheta_6^+\end{cases}\qquad \text{II:}\begin{cases}\vartheta_1 = \vartheta_1^-\\ \vartheta_2 = \vartheta_2^-\\ d_3 = d_3^-\\ \vartheta_4 = \vartheta_4^+\\ \vartheta_5 = \vartheta_5^+\\ \vartheta_6 = \vartheta_6^+\end{cases}\qquad \text{III:}\begin{cases}\vartheta_1 = \vartheta_1^+\\ \vartheta_2 = \vartheta_2^+ + \pi\\ d_3 = d_3^-\\ \vartheta_4 = \vartheta_4^+\\ \vartheta_5 = \vartheta_5^+\\ \vartheta_6 = \vartheta_6^+\end{cases}\qquad \text{IV:}\begin{cases}\vartheta_1 = \vartheta_1^-\\ \vartheta_2 = \vartheta_2^- + \pi\\ d_3 = d_3^+\\ \vartheta_4 = \vartheta_4^+\\ \vartheta_5 = \vartheta_5^+\\ \vartheta_6 = \vartheta_6^+\end{cases}$$

$$\text{V:}\begin{cases}\vartheta_1 = \vartheta_1^+\\ \vartheta_2 = \vartheta_2^+\\ d_3 = d_3^+\\ \vartheta_4 = \vartheta_4^-\\ \vartheta_5 = \vartheta_5^-\\ \vartheta_6 = \vartheta_6^-\end{cases}\qquad \text{VI:}\begin{cases}\vartheta_1 = \vartheta_1^-\\ \vartheta_2 = \vartheta_2^-\\ d_3 = d_3^-\\ \vartheta_4 = \vartheta_4^-\\ \vartheta_5 = \vartheta_5^-\\ \vartheta_6 = \vartheta_6^-\end{cases}\qquad \text{VII:}\begin{cases}\vartheta_1 = \vartheta_1^+\\ \vartheta_2 = \vartheta_2^+ + \pi\\ d_3 = d_3^-\\ \vartheta_4 = \vartheta_4^-\\ \vartheta_5 = \vartheta_5^-\\ \vartheta_6 = \vartheta_6^-\end{cases}\qquad \text{VIII:}\begin{cases}\vartheta_1 = \vartheta_1^-\\ \vartheta_2 = \vartheta_2^- + \pi\\ d_3 = d_3^+\\ \vartheta_4 = \vartheta_4^-\\ \vartheta_5 = \vartheta_5^-\\ \vartheta_6 = \vartheta_6^-\end{cases}$$

10 Conclusion

Along this essay it is possible to find several inverse kinematics solutions for robotic manipulators, following a geometrical approach. Simple planar geometries are addressed, as well as more complex structures, up to six degrees of freedom. The direct kinematics of robotic manipulators was also here addressed, through a brief review of the Denavit-Hartenberg convention and the respective construction of the reference frames.

References

[1] Needham, T. (1998). *Visual complex analysis*. Oxford University Press.

[2] Zwillinger, D. (Ed.) (2018). *CRC standard mathematical tables and formulas*, 33rd edition. Chapman and Hall/CRC.

[3] Siciliano, B., Sciavicco, L., Villani, L. and Oriolo, G. (2009), *Robotics: modelling, planning and control*. Springer-Verlag London Limited.

[4] Hartenberg, R. S., and Denavit, J. (1955). *A kinematic notation for lower pair mechanisms based on matrices*. Journal of Applied Mechanics.

[5] Spong, M. W., Hutchinson, S. and Vidyasagar, M. (2005). *Robot modeling and control*. John Wiley & Sons.

[6] Coxeter, H. S. M. and Greitzer, S. L. (1967). *Geometry revisited*. New Mathematical Library, Vol. 19, The Mathematical Association of America.

[7] Kucuk, S. and Bingul, Z. (2006), *Robot kinematics: Forward and inverse kinematics*. INTECH Open Access Publisher.